THE LUMPY CLUSTER ABELL 1185

ANDISHEH MAHDAVI, MARGARET J. GELLER, DANIEL G. FABRICANT, AND MICHAEL J. KURTZ

Harvard-Smithsonian Center for Astrophysics, 60 Garden Street, Cambridge, Massachusetts 02138
Electronic mail: amahdavi@rosat-mpe-garching.mpg.de, (mgeller, dfabricant, mkurtz)@cfa.harvard.edu

MARC POSTMAN AND BRIAN MCLEAN

Space Telescope Science Institute,[1] 3700 San Martin Drive, Baltimore, Maryland 21218
Electronic mail: (postman, mclean)@stsci.edu
Received 1995 September 5; revised 1995 October 10

ABSTRACT

Abell 1185, a richness class 1 cluster of galaxies ($c\bar{z} = 9800$ km s^{-1}), has kinematic and x-ray substructure. We measure 39 new velocities in its field, bringing the known cluster population to 82 galaxies within $1.4h^{-1}$ Mpc of the cluster center. The sample has a depth of $m_R \approx 15.8$, and no substantial spatial bias. In addition to the optical data we reanalyze a deep (11 459 s) Einstein x-ray observation. Clumps in the velocity distribution of A1185 are localized on the sky. The Dressler–Shectman test confirms the existence of subclumps with >99% confidence. X-ray emission from the cluster also appears complex; contributions from individual galaxies within A1185 are detectable. The brightest unresolved x-ray source coincides with an elliptical galaxy which contains an active LINER nucleus. Throughout the paper we define $H_0 = 100h$ km s^{-1} Mpc^{-1}, and unless otherwise indicated, we assume $h = 1$. © *1996 American Astronomical Society.*

1. INTRODUCTION

During the past decade we have witnessed a rapid increase in the sample of well-studied dynamically young clusters of galaxies (Dressler & Shectman 1988, hereafter referred to as DS88; Fitchett & Webster 1987; Fitchett 1988; Mohr *et al.* 1993; Henry & Briel 1995; den Hartog 1995; Mohr *et al.* 1995). These systems contain gravitationally bound subcondensations. Here we show that A1185 (Abell 1958) is a system where subclumping plays a significant role. We extend existing statistical tools for detecting substructure in optical (DS88) and x-ray (Soltan & Fabricant 1990, hereafter referred to as SF90) data.

Table 1 compares the results of previous studies of A1185 with our own. Hoessel *et al.* 1985 show that the brightest cluster galaxy (BCG) contains two nuclei with a separation of 3.2 kpc and $\Delta v = 58$ km s^{-1}. Rhee 1989 (hereafter referred to as R89) searches for substructure but finds none because he does not use radial velocities. He also fits a luminosity function to a set of R-band magnitudes. Zabludoff *et al.* 1993 (hereafter referred to as ZGHR93) include A1185 in their investigation of the distribution of cluster velocity dispersions.

In the x ray, Jones & Forman 1984 (hereafter referred to as JF84) and Rhee & Latour 1991 (hereafter referred to as RL91) fit surface-brightness profiles. JF84 also compute x-ray masses, and RL91 measure the ellipticity of the profile

---

[1]Space Telescope Science Institute is operated by the Association of Universities for Research in Astronomy, Inc., under contract to the National Aeronautics and Space Administration.

and the position angle, and find that the BCG is within one core radius of the x-ray center. We show, however, that the BCG has a peculiar velocity comparable to the cluster's global velocity dispersion. SF90, whose technique we adopt and extend, look for fluctuations in the x-ray emission profile of a large sample of Abell Clusters, and find fluctuations in A1185 at the 2σ level. We bin the same data for greater sensitivity, and supplement the x-ray observation with optical data.

We describe our observations and data reduction in Sec. 2, and determine cluster membership in Sec. 3. In Sec. 4 we show that A1185 has statistically significant structures in its velocity distribution, and that these structures are localized on the sky. We describe the x-ray data in Sec. 5, and in Sec. 6 we show that emission from individual galaxies contributes detectably to the total cluster emission. We summarize our findings in Sec. 7.

2. OBSERVATIONS AND DATA REDUCTION

Using Space Telescope Institute (STScI) scans of the Palomar Observatory Sky Survey (POSS), we select all galaxies with red-band $m_{STScI} \leq 16.0$ within a field of area 2.22° sq. This region corresponds to a circle of radius $1.4h^{-1}$ Mpc at the distance of A1185.

Because of plate-to-plate variations in the STScI instrumental magnitudes, and because our field crosses the boundary of two POSS plates, we calibrate the photometry using the Century Survey (Thorstensen *et al.* 1995). This redshift survey contains CCD-calibrated magnitudes of galaxies in a 102° sq. region which crosses the A1185 field. The resulting

TABLE 1. Properties of Abell 1185.[a]

	This Paper	ZGHR93	JF84	RL91, R89
Kinematic Properties				
R_{circ} (Mpc)	1.4	1.5	0.25	1[b]
N_z	82	69	...	5
$\bar{z}^{cluster}$	0.0326 ± 0.0003	0.0326 ± 0.0003	0.0349	0.0304
$\sigma^{cluster}_{uncor}$ (km s^{-1}) [c]	746	744	...	745
$\sigma^{cluster}$ (km s^{-1})	736($^{+65}_{-51}$)	718($^{+71}_{-55}$)	...	...
$\bar{z}^{0.25Mpc}$	0.0310 ± 0.0003	...	...	...
$\sigma^{0.25Mpc}$ (km s^{-1})	604($^{+125}_{-77}$)	...	...	...
X-Ray Properties[d]				
r_c (Mpc)	0.104 ± 0.06	...	0.035–0.205	0.05
β	0.58 ± 0.2	...	0.4–0.8	1
$L^{0.25Mpc}_X$ (10^{42} ergs s^{-1})[e]	5.5 ± 0.1	...	4.0 ± 0.2	...
$M^{1.5Mpc}_X$ ($M_\odot$)	...	...	4.1×10^{13}	...

[a]For consistency with the optical analysis we have transformed data from JF84 and RL91 to $H_0 = 100$ km s^{-1} Mpc^{-1}. In our column we list the optical properties of only the magnitude-limited sample. The ZGHR93 sample is not magnitude-limited; that of RKH89 is complete to $m_R = 18.0$ but has no velocity information. R_{circ} is the radius of the analysis region; N_z is the number of cluster members with redshifts.

[b]RKH89 use "an area large enough to include" 1 Mpc.

[c]See Danese *et. al.* 1980.

[d]We fit the β models after subtracting the eastern point source. RL90 assume $\beta = 1$ and hold it constant in their fits.

[e]Our value is bolometric; JF84 compute the 0.5–3.0 keV luminosity.

corrected magnitudes appear in Fig. 1. The dotted lines show the overlap region of the two POSS plates.

Vignetting effects decrease the POSS plate sensitivity near the boundaries; we minimize these effects by choosing our galaxy sample from the union of the two plates. The region of plate overlap contains 73% of the galaxies. The magnitude limit increases with distance (in R.A.) away from the center of the region, with a maximum deviation of 0.15 mag across the $2.8h^{-1}$ Mpc width of the field. The deviation is smaller than the average error in the calibrated magnitudes, $\sigma_{m_R} = 0.3$. The sensitivity does not vary with declina-
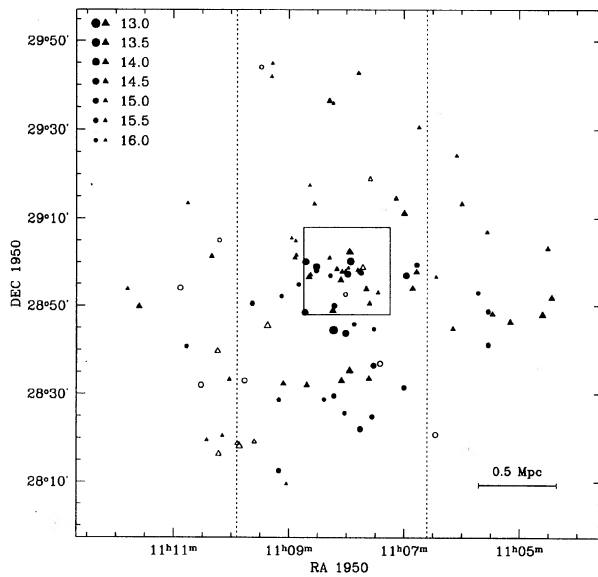

FIG. 1. Magnitude sky plot. The size of the points is proportional to their calibrated apparent magnitude. Triangles represent galaxies with previously measured redshifts; the circles are our new velocities. Filled points are cluster members: unfilled ones indicate foreground or background galaxies. The square shows the x-ray emitting region we consider in Sec. 5. The dotted lines contain the region where the Palomar plates overlap.

tion. The calibrated effective depth is $m_R \simeq 15.8$ for the entire field.

There are 101 galaxies with $m_R \leq 15.8$ within $1.4h^{-1}$ Mpc of the cluster center. For 62 of these we obtained velocities from the literature. During 1995 March we measured redshifts for the remaining 39 galaxies using the FAST spectrograph (Fabricant 1994) on 1.5 m Tillinghast reflector on Mt. Hopkins, Arizona. Exposures were 5–10 min for spectra covering the wavelength range 4000–7500 Å. We compute redshifts with XCSAO (Kurtz *et al.* 1992), which employs cross-correlation techniques on log-wavelength binned spectra (Tonry & Davis 1979). Velocity errors are approximately 40 km s^{-1}. Table 2 lists velocities for our sample; * indicates new measurements.

3. CLUSTER MEMBERSHIP

The histogram in Fig. 2(a) shows the previous velocity measurements (shaded bars), and our new ones (white bars). The large peak near 9800 km s^{-1} is clearly the cluster. We determine the cluster membership using the method outlined in Zabludoff *et al.* 1993. First, we remove all galaxies more than 2000 km s^{-1} from the nearest galaxy in the peak. For this newly defined "test sample," we compute the velocity dispersion σ and the mean $\bar{v}$. We then rank the right-hand and left-hand peculiar velocities

$$r_i = |v_i - \bar{v}|, \quad v_i > \bar{v}, \quad r_i > r_{i-1};$$
$$l_j = |v_j - \bar{v}|, \quad v_j < \bar{v}, \quad l_j > l_{j-1}. \tag{1}$$

Then we find the smallest i,j such that

$$r_i - r_{i-1} > \sigma,$$
$$l_j - l_{j-1} > \sigma. \tag{2}$$

We remove all galaxies with $r_{\geq i}$, $l_{\geq j}$ from the test sample, recompute σ and $\bar{v}$, and repeat the procedure until no galaxy satisfies conditions (2).

By applying this procedure to our galaxy sample, we find 82 cluster members for A1185; of these, 31 are the results of our new spectroscopy. The total foreground/background contamination (19 galaxies) is consistent with the expected number

$$N_{nonmember} = 2.2 \times \int_{-\infty}^{15.8} C_0 10^{d_0 m} \, dm$$
$$= 18, \tag{3}$$

for a uniform background determined from the Century Survey, where $d_0 = 0.610 \pm 0.005$ and C_0 yields 3.67 ± 0.08 galaxies per magnitude per square degree at $m_R = 15.0$.

4. VELOCITY SUBSTRUCTURE

Figure 2(b) shows the 82 member galaxies. The bins in this histogram are 250 km s^{-1}, five times a pessimistic estimate of the average error in the velocities. The distribution appears to have structure: three peaks at approximately 8500,

TABLE 2. The magnitude-limited redshift sample.

Cluster Members

RA (1950)	DEC (1950)	v (km s^{-1})	Source
11:04:26.5	28:51:45	10155	a
11:04:30.6	29:03:08	9587	b
11:04:36.1	28:47:53	9987	b
11:05:09.6	28:46:14	9800	a
11:05:28.2	28:48:04	9462	a
11:05:32.6	28:48:42	9584	*
11:05:32.7	28:41:05	9777	*
11:05:33.9	29:06:51	9303	c
11:05:43.1	28:52:55	9562	*
11:06:00.0	29:13:15	10281	c
11:06:09.3	28:44:46	10976	b
11:06:27.0	28:56:35	9735	b
11:06:47.0	28:59:23	9614	*
11:06:47.3	28:57:43	9847	b
11:06:51.3	28:53:55	11619	b
11:06:57.9	28:56:56	11320	*
11:06:59.8	29:11:09	9624	c
11:07:00.1	28:31:25	9351	*
11:07:08.4	29:14:32	9658	c
11:07:27.3	28:52:59	9278	b
11:07:31.6	28:44:42	11099	*
11:07:32.1	28:36:25	10346	*
11:07:33.5	28:24:50	10482	*
11:07:36.2	28:50:32	9268	b
11:07:36.9	28:33:28	9943	b
11:07:39.5	28:53:50	11528	b
11:07:45.0	28:57:30	9582	*
11:07:45.5	28:57:57	8923	b
11:07:45.8	28:22:03	10755	*
11:07:47.7	29:42:44	8565	c
11:07:48.4	28:58:12	9738	b
11:07:52.3	28:45:49	10701	*
11:07:55.8	29:00:13	9317	*
11:07:56.9	28:35:16	10393	d
11:07:56.9	29:02:23	(BCG) 10521	a
11:07:58.2	28:58:41	8579	e
11:07:59.0	28:57:17	9765	*
11:08:01.0	28:43:45	9852	*
11:08:01.2	28:57:51	9988	b
11:08:02.0	28:25:39	10375	*
11:08:04.8	28:57:49	9769	b
11:08:05.2	28:32:58	10767	e
11:08:06.2	28:55:52	8741	b
11:08:10.3	28:58:25	10192	b
11:08:12.8	28:50:00	9426	*
11:08:13.2	28:29:34	10685	*
11:08:13.8	28:44:27	9511	*
11:08:14.0	29:35:57	8837	c
11:08:14.3	28:48:53	9606	a
11:08:17.0	28:56:55	9210	*
11:08:17.8	29:00:59	9809	c
11:08:18.0	29:36:27	8730	c
11:08:23.5	28:28:45	9505	*
11:08:31.5	28:58:58	8853	*
11:08:31.6	28:58:03	(LINER AGN) 8754	*
11:08:33.6	29:13:15	9039	c
11:08:37.7	28:57:07	8826	b
11:08:38.4	29:17:31	9285	c
11:08:39.3	28:56:34	8717	b
11:08:41.6	28:31:59	10652	a
11:08:42.6	29:00:06	9576	*
11:08:43.5	28:48:31	9161	*
11:08:50.0	28:54:51	8539	*
11:08:52.6	29:01:35	9498	c
11:08:53.2	29:04:50	9520	c
11:08:53.8	29:01:00	8564	b
11:08:57.4	29:05:29	9792	c
11:09:02.6	28:09:30	10574	b
11:09:05.9	28:32:19	10759	b
11:09:07.8	28:52:10	9753	*
11:09:10.5	28:28:39	9391	*
11:09:10.6	28:12:33	10590	*
11:09:17.2	29:44:57	10240	c
11:09:18.0	29:41:56	8653	c
11:09:38.4	28:50:31	10002	*
11:10:02.2	28:33:15	10475	c
11:10:09.3	28:20:31	10248	a
11:10:20.4	29:01:19	8719	c
11:10:45.3	29:13:28	10255	c
11:10:46.6	28:40:46	10357	*
11:11:36.0	28:49:49	10306	b
11:11:48.1	28:53:46	10565	c

Foreground/Background Galaxies

RA (1950)	DEC (1950)	v (km s^{-1})	Source
11:06:05.4	29:24:10	23527	b
11:06:27.5	28:20:50	13947	*
11:06:44.6	29:30:29	14140	c
11:07:25.2	28:36:52	13962	*
11:07:35.4	29:18:56	7512	c
11:07:43.2	28:58:45	21177	c
11:08:01.2	28:52:37	22079	*
11:09:22.4	28:45:27	1554	b
11:09:28.8	29:44:04	23950	*
11:09:36.1	28:19:09	14141	b
11:09:46.3	28:32:58	14179	*
11:09:51.7	28:18:08	14141	a
11:09:53.8	28:18:46	13803	b
11:10:12.5	29:05:00	31555	*
11:10:13.2	28:16:21	14012	b
11:10:14.4	28:39:42	6404	a
11:10:25.6	28:19:30	6416	b
11:10:31.5	28:31:58	14208	*
11:10:53.2	28:54:03	19028	*

Vvelocity errors are ± 40 km s^{-1}.

Sources: *—This paper; a—Zabludoff *et. al.* 1993; b—Huchra *et. al.* 1995; c—Thorstensen *et. al.* 1995; d—de Vaucouleurs *et. al.* 1976; e—Hamwey 1987

9500, and 10 500 km s^{-1}, and a high-velocity tail at 11 500 km s^{-1}. We refer to these apparent structures as P_1, P_2, P_3, and P_4, respectively.

Figure 3 shows qualitative evidence for kinematic sub-structure in A1185. The division of the velocity peaks is somewhat arbitrary, but P_2 is clearly the core, and P_1 and P_3 seem segregated on the sky. To evaluate the significance of this apparent kinematic substructure, we employ a test devel-
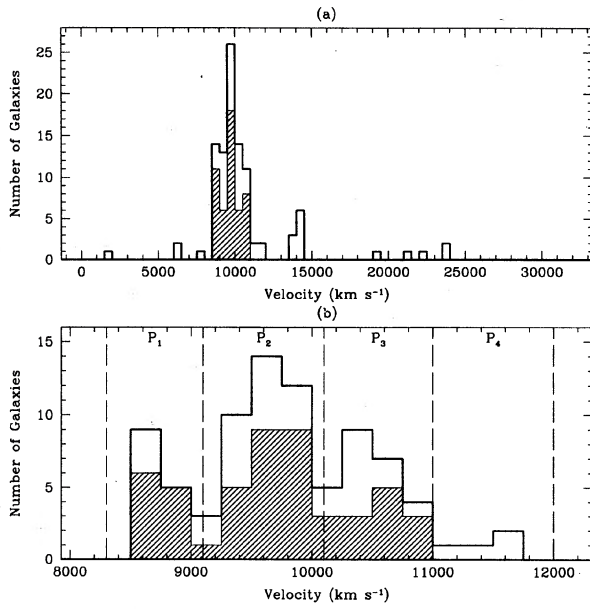
FIG. 2. Velocity Histograms. The distribution of velocities for the entire field (a), and the cluster members only (b). Shaded bars indicate velocities from the literature, and the unshaded portions of the histogram are our new measurements.
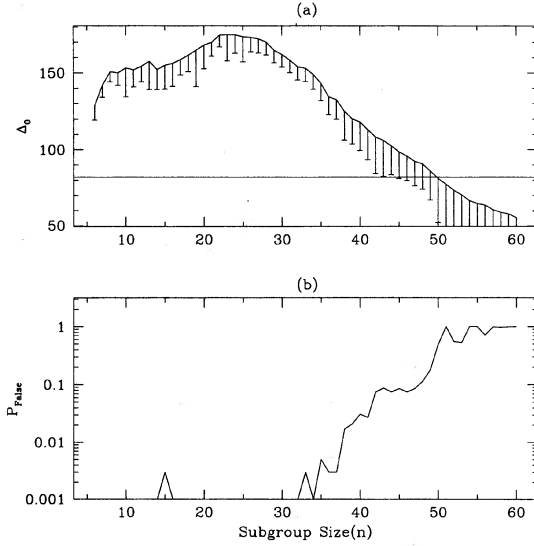

FIG. 4. The Dressler–Shectman statistic as a function of n. (a) shows the value of Δ_0, computed for the true cluster A1185, as a function of the small group size. The error bars show the 68% confidence interval. The straight line shows $\Delta_0=N=82$, below which Δ_0 is *a priori* not significant. (b) shows P_{False}, the probability that Δ_0 is large by accident, garnered from 500 Monte Carlo simulations of the cluster.

oped by Dressler & Shectman 1988 (DS88). For each of the N_{tot} members of a cluster, we find the nearest $n-1$ galaxies to form a subgroup of size n. For each subgroup we compute the deviation statistic

$$\delta_i^2 \equiv \frac{n}{\sigma_0^2} \left[(\bar{v}_i - \bar{v}_0)^2 + (\sigma_i - \sigma_0)^2 \right], \tag{4}$$

where $\bar{v}_0$ and σ_0 are the mean velocity and dispersion for the cluster, and $\bar{v}_i$ and σ_i are the same quantities for the subgroup. The value of δ_i measures the deviation of the subgroup's local kinematics (indicated by $\bar{v}_i$ and σ_i) from the global kinematics of the entire cluster ($\bar{v}_0$ and σ_0). The sum of all the local deviations,

$$\Delta_0 \equiv \sum_{i=1}^{N_{\text{tot}}} \delta_i, \tag{5}$$

is a measure of the degree of substructure in the cluster. There is an uncertainty in Δ_0, $\epsilon(\Delta_0)$, which arises from measurement errors in σ and $\bar{v}$. We compute these latter errors using the procedure outlined in Danese *et al.* 1980, and derive ϵ by applying Gaussian error propagation. Again, we use a pessimistic estimate of the velocity measurement errors (50 km s^{-1}).

A large value of Δ_0 is only a preliminary indicator of significant substructure. The Δ statistic requires calibration by shuffling all the velocities a large number M times, keeping the sky positions constant. This Monte Carlo technique yields M simulated values of Δ. A conservative estimate of the probability that the observed Δ_0 is large as a result of statistical fluctuations is

$$P_{\text{False}} = \frac{N_{\text{sim}} > \Delta_0^{1\sigma}}{M}, \tag{6}$$

$$\Delta_0^{1\sigma} \equiv \Delta_0 - \epsilon(\Delta_0), \tag{7}$$

where $\epsilon(\Delta_0)$ is the 68% confidence uncertainty in Δ_0. In other words, P_{False} is the fraction of simulations that had $\Delta_{\text{sim}} > \Delta_0^{1\sigma}$. A very small P_{False} means that $\Delta_0 \gg N$ is significant, which in turn is an indicator that deviations from the cluster's global kinematics are localized.

FIG. 3. Galaxy positions associated with the four velocity peaks. The shaded portion of the velocity histogram is the peak shown in each plot.
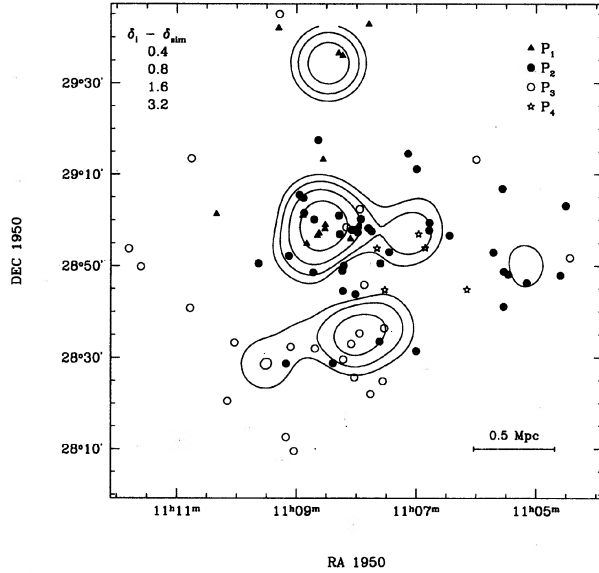
FIG. 5. Local contributions to the Dressler–Shectman statistic for $n = 6$. The contour plot shows $\delta(x,y)$ after Monte Carlo calibrations. As in Eq. (4), δ is in units of the global velocity dispersion. The positions x and y, are the mean R.A. and DEC of the n-member subgroup, weighted by each galaxy's contribution to that δ. The various graphical symbols correspond to galaxies in P_1–P_4 (see Fig. 2).
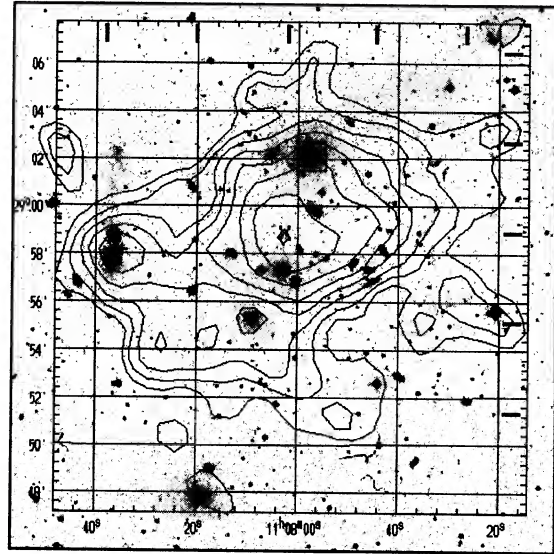

FIG. 6. The x-ray profile of A1185. We have background subtracted the data, correcting for the Einstein IPC vignetting effects and smoothing by the IPS PSF. The first contour corresponds to a surface brightness of 4.4 counts arcmin^{-1} or 1.7×10^{43} ergs s^{-1} Mpc^{-2}, the 3σ detection level. Contours then increase logarithmically to 32 counts arcmin^{-1} or 1.2×10^{44} ergs s^{-1} Mpc^{-2}. The cross marks the position of the x-ray center, the plus sign ("+") locates the eastern peak. A small square marks the BCG.

Figure 4 shows the results of the Dressler–Shectman test as a function of n, the small group size. We use $M = 500$ for the calibrations, and vary n from 6 to 60 (DS88 use $n = 11$) for a total of 27 500 simulations. Over the 12 500 simulations in the range $n = 6$–30, $\Delta_{sim} > \Delta_0^{1\sigma}$ only once. The range where Δ_0 is large and significant is a measure of the size of the kinematic substructures.

Figure 5 is a contour plot of $\delta(x,y)$ for $n = 6$. As mentioned above, the values of δ require calibration; we have subtracted $\delta_{sim}(x,y)$ (the average values of δ_i for the $M = 500$ Monte Carlo simulations of this cluster) and display the residuals. The peaks in this function are the chief contributors to the large value of the Δ_0 statistic.

These plots support the qualitative impression drawn from Fig. 3. The southern peak in Fig. 5 includes galaxies belonging to P_3, and the larger central peak and the northern peak coincide with galaxies in P_1. The Dressler–Shectman test confirms substructure in A1185 at better than the 99% confidence level. Note that the substructures lie primarily along the declination axis, and are therefore insensitive to the 0.15 mag, R.A.-directed gradient in the limiting magnitude of the survey.

5. THE X-RAY DATA

The Einstein Satellite's Imaging Proportional Counter (IPC, sensitive in the 0.16–3.5 keV energy band) observed A1185 for 11 459 s on 1980 May 16. Table 1 lists the x-ray properties of the cluster; for comparison we also provide some values computed for A1185 by Jones & Forman 1984 (JF84) and Rhee & Latour 1991 (RL91). David *et al.* 1993 report an x-ray temperature of 2.8–5.9 keV.

Figure 6 shows a contour plot of the x-ray emitting region, superimposed upon an STScI scan of the POSS. This region corresponds to the small square in Fig. 1. The first contour represents emission at a level 3σ above the background. We have binned the original 8" pixels into 32" pixels, and smoothed the image with a Gaussian approximation to the point spread function (PSF). The approximate PSF has $\sigma \sim 38"$, which at the distance of A1185 corresponds to $18h^{-1}$ kpc.

We first turn our attention to the secondary peak to the east of the main one. Its center, computed using luminosity-weighted moments and marked with a "+," is superposed upon two bright galaxies. To measure its extent, we fit its profile to a two-dimensional Gaussian. Assuming Poisson errors for the data points, χ^2/ν (see Press *et al.* 1994, Sec. 14.1) is 1.67. The resulting $\sigma = 38.4" \pm 14"$ is indistinguishable from the IPC PSF with $\sigma = 38"$. The centroid of this peak is $\sim 40"$ from either galaxy, and is consistent with the galaxy positions within the statistical and systematic errors.

We obtain the total x-ray luminosity of this eastern peak by integrating the analytic form of the best-fit PSF. The resulting value, $6 \pm 0.5 \times 10^{40}$ ergs s^{-1}, is about 1% of the total bolometric x-ray luminosity of the cluster.

The optical spectrum of the southern elliptical galaxy (Fig. 7, from the FAST spectrograph) is consistent with that of low-ionization nuclear emission-line regions (LINERs; Heckmann 1980 (hereafter referred to as H80). This spectrum satisfies all of H80's line strength criteria for LINERs: [O II]$\geq$[O III]; [O I]$\geq \frac{1}{3}$[O III]; furthermore, [N II]>0.6 Hα, an additional property peculiar to most LINERs in elliptical galaxies (see Ho *et al.* 1993).
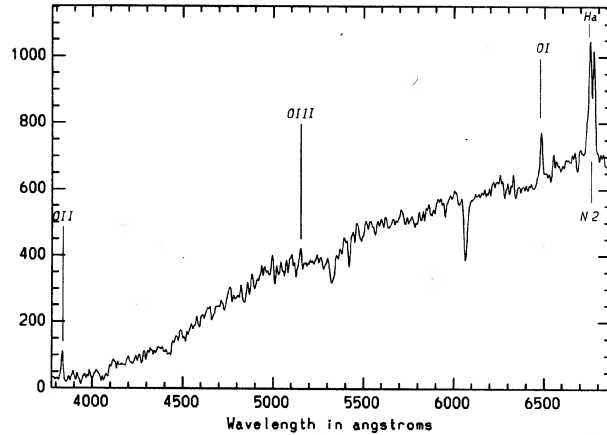
FIG. 7. The spectrum for NGC 3561s. NGC 3561s is the southern of the two galaxies coincident with the eastern x-ray peak. The spectrum shows the properties of a LINER.

LINERs typically have x-ray luminosities between $\log L_X \sim 39.3-41.4$ ($h=1$) (Fabbiano 1995), consistent with the total luminosity of the eastern peak. The northern candidate is a spiral; x-ray emission for normal spirals is typically $\log L_X = 37.4-39.4$ (Fabbiano *et al.* 1984). In view of these luminosity ranges, it is likely that the LINER dominates x-ray emission from the eastern peak.

In what follows we remove the eastern point source from the image, obtaining the map in Fig. 8. This plot also displays the size of the x-ray core radius in the β-model profile:

$$S = S_0 \left(1 + \frac{r^2}{r_c^2} \right)^{-3\beta+1/2}. \tag{8}$$

We perform a three-parameter minimization of the chi-square statistic, and find $\beta = 0.104 \pm 0.06$ and $r_c = 0.58 \pm 0.2$ Mpc; χ^2/ν is 0.34. Our values agree with JF84; RL91 assume $\beta = 1$ for all their clusters.

The cross "$\times$" in this figure indicates the x-ray center of the cluster, computed using the luminosity weighted moments of the image. The first rank or brightest cluster galaxy (BCG) is $\sim r_c$ from the x-ray center, in agreement with RL91. However, the BCG has a large peculiar velocity: it belongs to P_3, with $v_{BCG} - \bar{v}_0 = 753 \pm 70$ km s$^{-1} \sim \sigma_0$. Because its velocity differs from the mean velocity of the cluster by an amount comparable with the global velocity dispersion, we conclude that the BCG is probably not associated with the center of the cluster potential well.

6. FLUCTUATIONS IN THE DIFFUSE X-RAY EMITTING GAS

If individual galaxies other than the LINER contribute significantly to the total cluster x-ray emission, these contributions should appear as fluctuations in the smooth profile in Fig. 8. However, such fluctuations could also arise from background sources and instrumental effects. Soltan & Fabricant 1990 (SF90) develop a method for detecting significant "lumpiness" in excess of these latter effects.

Using a best-fit β model for a given cluster, SF90 construct a large number of simulated observations, including
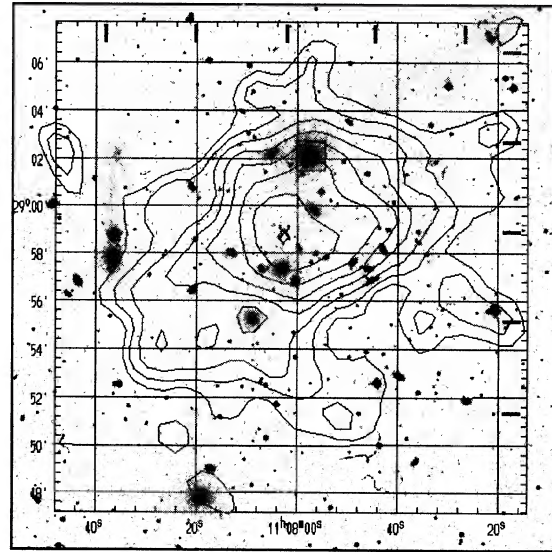

FIG. 8. The x-ray profile of A 1185 after the subtraction of the eastern peak. We remove the peak marked with a "+" in Fig. 6 by replacing a circular area of radius $3'' \times 38''$ with an average of its neighboring pixels. We use this profile for subsequent analysis. Each tick marks one core radius; the small square contains the BCG.

statistical noise, instrumental modulations peculiar to the IPC, and foreground/background sources. The flux distribution of the background sources is taken from Gioia *et al.* 1984 and Gioia *et al.* 1990.

To test for statistically significant fluctuations within a particular region, SF90 compute the mean square pixel-by-pixel difference between the best-fit β model and each of the simulations:

$$F \equiv \sum_{i=1}^{N} \frac{[\text{counts(model)} - \text{counts(pixel}_i)]^2}{N-1}, \tag{9}$$

where N is the total number of pixels in the region. For each pixel, r_c and β are constant, but S_0 is fit to reflect the features of the local profile, in order to prevent large-scale gradients from contributing to F. Fluctuations likely due to cluster galaxies are detectable if the fluctuation statistic F_0 of the observed cluster is greater than a large fraction (SF90 use 95%) of the fluctuations computed for the simulated clusters.

SF90 bin the x-ray data spatially into $64''$ pixels, and use a series of nonoverlapping annuli as their analysis regions. For A1185 they find fluctuations at the 2σ level above the expected Poisson fluctuations. They do not remove the unresolved source to the east, which we discuss above, but the fluctuations are detectable at smaller radii.

We bin the data into $32''$ pixels. Our fluctuations are consistent with those of SF90 in the same annuli. However, we also compute a cumulative distribution of fluctuations as a function of radius [Fig. 9(a)]. Our analysis region is always a circle of radius r from the cluster center, omitting an inner circle of radius 2 pixels ($0.25r_c$) in order to leave out large fluctuations introduced by the core.
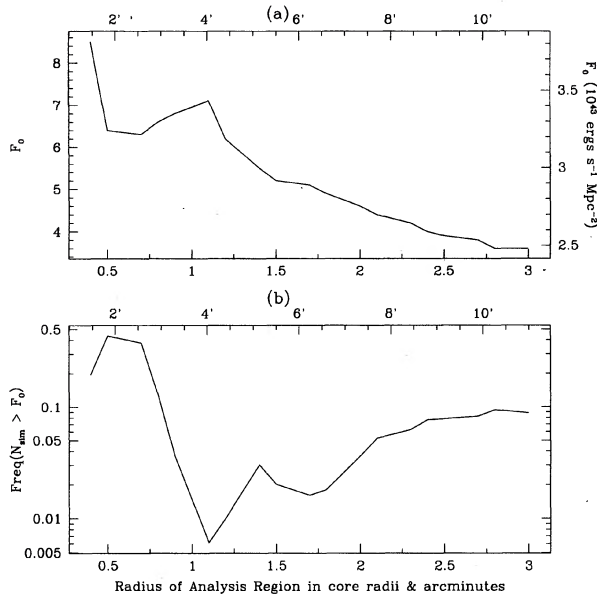
FIG. 9. The *Einstein* IPC observation of A1185 is only marginally consistent with a β model including background sources, statistical fluctuations, and instrumental modulations. (a) shows the cumulative mean pixel-by-pixel deviation of A1185 from its best-fit β model. (b) displays the fraction of our 500 simulated clusters which show more fluctuations than the real cluster. Over $r_c < r < 2r_c$, the fraction is ~3%.

The results of our 500 simulations appear in Fig. 9(b), where we plot the frequency of simulated clusters with fluctuations greater than F_0. In the region between r_c and $2r_c$, well outside the brightest central region, yet still within the 3σ x-ray detection contour, the observation is lumpier than 97% of the simulations. Thus A1185 is only marginally consistent with a pure β model emitting with coincident background sources. This result is a slight improvement of SF90's 2σ detection, because looking at fluctuations in cumulatively larger regions reduces the amplitude of the Poisson noise which dominates the total fluctuations.

Figure 10 traces the contributions of individual pixels to F_0. The contours measure the square deviation of each pixel from the value predicted for that pixel by the β model.

We now use the SF90 technique to place an upper limit on emission from galaxies in A1185. To construct a model, we place unresolved x-ray sources at the positions of galaxies within the desired region. Then we add a β model modified so that the total x-ray luminosity of the cluster remains constant. Finally, we supply the instrumental modulations and statistical noise.

We already have positions for galaxies with $m_R \leq 15.8$. We obtain additional galaxies with $m_R \leq 16.8$ by using the Faint Object Classification and Analysis System (FOCAS; Tyson 1990; Valdes *et al.* 1993) on POSS scans by the STScI. We calibrate our magnitudes using the Century Survey, applying the same method as in Sec. 2. This technique yields 16 galaxies with $m_R \leq 15.8$ and 21 galaxies with $15.8 \leq m_R \leq 16.8$ within the region $0 \leq r \leq 2r_c$. We limit our investigation to $2r_c$ to remain within the limits of 3σ x-ray isophote. Over this isophote POSS plate effects are negligible. Approxi-
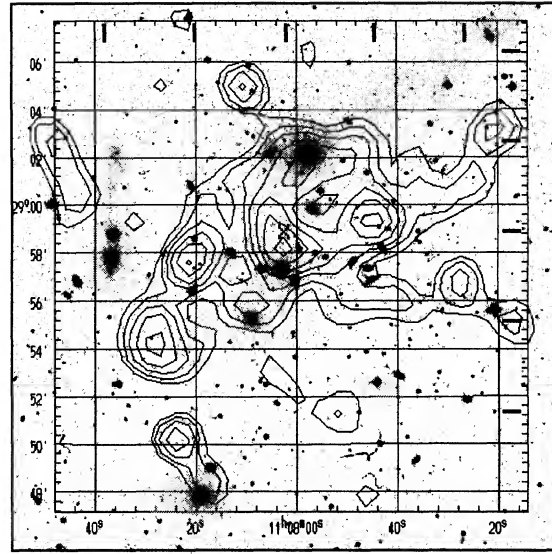

FIG. 10. Fluctuation map for A1185. The contour map shows the pixel-by-pixel deviation of the cluster x-ray profile from the best-fit β model. The lowest contour corresponds to a surface-brightness fluctuation of 2.2×10^{43} ergs s^{-1} Mpc^{-2}, proceeding logarithmically up to 5.1×10^{43} ergs s^{-1} Mpc^{-2}. The peaks in the fluctuations show some correspondence with the positions of individual galaxies. Each tick marks one core radius.

mately 1 of the faintest 21 sources should be a background galaxy.

We run three sets of 500 simulations each, including the 37 $m_R \leq 16.8$ galaxies. In each of the 1500 simulations, we assign every galaxy an x-ray luminosity randomly drawn
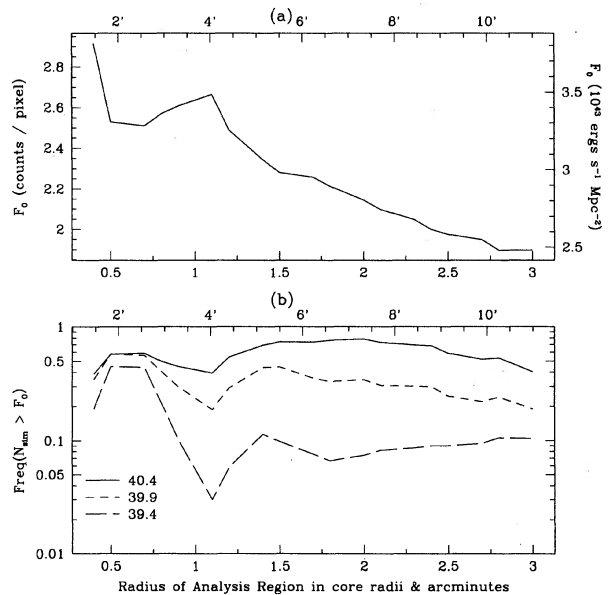

FIG. 11. Constraining the mean point-source emission in A1185. (a) is the same as Fig. 9(a). (b) shows the fraction of 500 simulated clusters with more fluctuations than the real cluster, as a function of radius and mean log x-ray emission (three curves with mean log x-ray emission as indicated on the plot).

from a normal distribution with mean $\log L_X = 39.4$ (set 1), 39.9 (set 2), or 40.4 (set 3) in ergs s^{-1}; the log standard deviation is 0.6 for all sets. The third set, lot $L_X = 40.4$ ($h = 1$), corresponds to the mean emission of a sample of field E and S0 galaxies from Eskridge *et al.* 1995 (hereafter referred to as EFK95). The mean emission for the two other simulations is simply a decrement of $\log L_X = 0.5$.

Figure 11 shows the results of all three sets of simulations. Outside r_c, fewer than 10% of the simulations with point sources at $\log L_X = 39.4$ show more fluctuations than the data.

However, about 50%–70% of the simulations at $\log L_X = 40.4$ show more fluctuations than the cluster, while at $\log L_X = 39.9$ the range is 20%–50%. Thus the Einstein IPC observation of A1185 is consistent with a β model coincident with background sources, instrumental modulations, statistical fluctuations, and galaxies emitting at mean $\log L_X$ between 39.9 and 40.4 (in ergs s^{-1}). We therefore cannot rule out emission from all the cluster galaxies at the EFK95 value for field ellipticals.

7. CONCLUSION

We have measured 39 velocities within $1.4h^{-1}$ Mpc of the field center of Abell 1185 in order to construct a redshift sample with an effective depth of $m_R \simeq 15.8$. There are 82 cluster members and 19 foreground and background galaxies in the region. The velocity distribution of the members shows evidence of kinematic substructure, which the Dressler–Shectman test verifies at better than the 99% confidence level. The substructure identified by the test is localized on the sky.

The subclumps in A1185 make it problematic to compute a virial mass for the whole system. Even within $0.25h^{-1}$ Mpc of the cluster center there is superposed substructure from three subclumps; the velocity dispersion σ (0.25 Mpc) is comparable to the global velocity dispersion. Any measurement of a virial mass for this dynamically young system is likely to be a serious overestimation; we do not attempt it. The x-ray mass computed by JF84 ($4.1 \times 10^{13}\ \mathscr{M}_\odot$ within 1.5 Mpc, $h = 1$) is likely to be a more robust estimate.

There is evidence for x-ray substructure. An unresolved source distinct from the intracluster gas is coincident with an elliptical galaxy containing a LINER. Statistical test devised by SF90 show that the smooth emission profile may contain (at the 97% confidence level) fluctuations due to factors other than noise, instrumental modulations, and background sources. Further simulations show that the cluster is consistent with emission from the individual galaxies at a level comparable with that of field ellipticals.

REFERENCES

Abell, G. 1958, ApJS, 3, 211
Danese, L., De Zotti, G., & Tullio, G. 1980, A&A, 82, 322
David, L., Slyz, A., Jones, C., Forman, W., Vrtilek, S., & Arnaud, K. 1993, ApJ, 412, 479
den Hartog, R., 1995, Ph. D. thesis, Leiden University
Dressler, A., & Shectman, S. 1988, AJ, 95, 985
Eskridge, P., Fabbiano, G., & Kim, D. 1995, ApJ, 97, 141
Fabbiano, G., Trinchieri, G., & MacDonald, A. 1984, ApJ, 284, 65
Fabbiano, G. 1995 (private communication)
Fabricant, D. 1994, Technical Report, Harvard-Smithsonian Center for Astrophysics
Fitchett, M., & Webster, R. 1987, ApJ, 317, 653
Fitchett, M. 1988, MNRAS, 230, 161
Gioia, I., Maccacaro, T., Schild, R., Stocke, J., Liebert, J., Danziger, I., Kunth, D., & Lub, J. 1984, ApJ, 283, 495
Gioia, I., Maccacaro, T., Schild, R., Wolter, A., Stocke, J., Morris, S., & Henry, J. 1990, ApJS, 72, 567
Henry, J., & Briel, U. 1995, ApJ, 443, 9
Hoessel, J., Kirk, D., & Schneider, D. 1985, ApJ, 293, 94
Hamwey, R. 1987, Ph. D. thesis, Dartmouth College
Heckmann, T. 1980, A&A, 87, 152
Ho, L., Flippenko, A., & Sargent, W. 1993, ApJ, 417, 63
Huchra, J., Geller, M., Clemens, C., & Tokarz, S. 1995, The Center for Astrophysics Redshift Catalog, Harvard-Smithsonian Center for Astrophysics, Cambridge, MA 02138

Jones, C., & Forman, W. 1984, ApJ, 276, 38
Kurtz, M., Mink, D., Wyatt, W., Fabricant, D., Torres G., Kriss, G., & Tonry, J. 1992, in Astronomical Data Analysis Software and Systems, edited by D. Worrall, C. Biemesderfer, and J. Barnes, ASP Conf. Ser. (ASP, San Francisco), p. 232
Mohr, J. Evrard, A., Fabricant, D., & Geller, M. 1995, ApJ, 447, 8
Mohr, J., Fabricant, D., & Geller, M. 1993, ApJ, 413, 492
Press, W., Flannery, B., Teukolsky, S., & Vetterling, W. 1994, Numerical Recipies (Cambridge University Press, New York)
Rhee, G. 1989, Ph. D. thesis, Rijksuniversiteit Leiden
Rhee, G., & Latour, H. 1991, A&A, 243, 38
Soltan, A., & Fabricant, D. 1990, ApJ, 364, 433
Thorstensen, J., Wegener, G., Geller, M., Kurtz, M., Fabricant, D., Huchra, J., Marzke, R., & Schild, R. 1995, in preparation
Tonry, J., & Davis, M., 1979, AJ, 84, 1511
Tyson, J. A., 1990 in Proceedings of the Edwin Hubble Centennial Symposium (Astronomical Society of the Pacific, Berkeley, CA), p. 292
Valdes, F., Abraham, R., Van Den Bergh, S., & Yee, H. 1993, BAAS, 183, #03.09
de Vaucouleurs, G., de Vaucouleurs, A., & Corwin, H. 1976, The Second Reference Catalogue of Bright Galaxies (University of Texas Press, Austin)
Zabludoff, A., Geller, M., Huchra, J., & Vogeley, M. 1993, AJ, 106, 1273
Zabludoff, A., Geller, M., Huchra, J., & Ramella, M. 1993, AJ, 106, 1301